# Early Transition Metal Complexes of Triphosphorus Macrocycles

**Robert J. Baker,[a] Philip C. Davies,[a] Peter G. Edwards,*[a] Robert D. Farley,[a] Sudantha S. Liyanage,[a] Damien M. Murphy,[a] and Ben Yong[a]**

**Keywords:** Macrocyclic ligands / P ligands / Titanium / Vanadium / Chromium

The reactions of 1,5,9-triethyl-1,5,9-triphosphacyclododecane, [12]ane$P_3Et_3$, with first-row transition metal halides $MCl_3$ [M = Ti (**1**), V (**2**), and Cr (**3**)] or their THF adducts are reported. The oxidation of **2** gives the complex ([12]ane$P_3Et_3$)-$V(O)Cl_2$ (**4**). This is the first example of a phosphane ligand that is *trans* to a vanadyl moiety. Also reported are $V^{III}$ (**5**) and $Cr^{III}$ (**6**) complexes of the pendant ether macrocycles [12]ane$P_3(C_2H_4OEt)_3$ and 12[ane]$P_3(C_3H_6OMe)_3$ respectively. The complexes **1**–**6** have been characterised crystallographically and represent a rare class of phosphane complexes of these metals. The paramagnetic $d^1$ compounds are characterised by EPR and ENDOR spectroscopy, simulation of which gives valuable structural information of these species in frozen solution. With [12]ane$P_3Et_3$, $Nb^{III}$ and $Nb^{IV}$ chlorides give air-sensitive materials which could not be fully characterised although by comparison with compound **4**, EPR and ENDOR spectroscopy indicate the principal oxidation product to be ([12]ane$P_3Et_3$)$Nb(O)Cl_2$ (**7**).


## Introduction

Phosphane ligands are known to readily form complexes with late transition metals. Phosphane complexes of the early transition metals, however, are still relatively uncommon and less well studied; this being predominantly due to inherent kinetic lability that limits the opportunity to obtain discrete and well-behaved complexes for further studies. The understanding of appropriate reaction conditions has led to a resurgence of interest in this field.[1] The majority of phosphane complexes of group-5 metals are stabilised by metal−metal interactions.[2] In view of the intrinsic lability of phosphane complexes of these electropositive metals, and the observation that the majority of organometallic derivatives of group-4 and -5 metals are stabilised by cyclopentadienyl and related ligands,[3] we have chosen to take advantage of the macrocyclic coordination effect and to study the coordination chemistry of 1,5,9-trialkyl-1,5,9-triphosphacyclododecane ([12]ane$P_3R_3$) macrocycles with early transition metals. These phosphane macrocycles[4] also bear a resemblance to the cyclopentadienyl family of ligands in that they can be considered to coordinate in a 6-electron, facial tridentate fashion. Thus the reactivity of complexes of these ligands will be of interest. In this paper we will describe the chemistry of group-4 and -5 metals with [12]ane$P_3R_3$ ligands and some related chemistry of chromium.

## Results and Discussion

### $M^{III}$ Complexes (M = Ti, V, Cr)

Complexes of [12]ane$P_3Et_3$ (1,5,9-triethyl-1,5,9-triphosphacyclododecane) are readily formed by the addition of the ligand to a dichloromethane solution of $MCl_3$·3THF and are obtained as light blue (Ti), green (V) and blue (Cr) paramagnetic solids. The new compounds and their syntheses are outlined in Scheme 1. The chromium complex is also an intermediate in the synthesis of free [12]ane$P_3Et_3$ and may be formed by halogen oxidation of the $Cr(CO)_3$ adduct.[4]

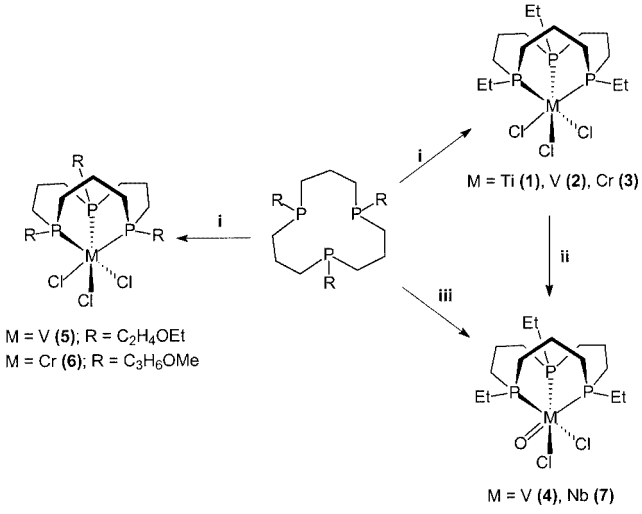


Scheme 1. i) $MCl_3(THF)_3$, $CH_2Cl_2$; ii) air, $CH_2Cl_2$; iii) $NbCl_3$(DME), air, $CH_2Cl_2$

[a] Department of Chemistry, Cardiff University,
P. O. Box 912, Cardiff, CF10 3TB, U.K.
E-mail: EdwardsPG@cardiff.ac.uk

The reaction of [12]ane$P_3Et_3$ with solutions of $TiCl_3$·3THF causes an immediate colour change to pale blue, and crystalline **1** can be isolated in good yield. Analytical and mass spectrometric data are consistent with the formula ([12]ane$P_3Et_3$)$TiCl_3$, and the magnetic susceptibility indicates a $d^1$ paramagnet. The crystal structure of **1** is shown in Figure 1 and selected bond lengths and angles are given in Table 1. The structure shows the expected octahedral geometry at the metal centre with the macrocycle capping one face. The complex shows a weak Jahn−Teller distortion, as expected for $d^1$ $Ti^{III}$. Although the quality of structural data is poor, one titanium−phosphorus bond appears marginally longer than the other two [2.623(4) Å compared to 2.608(4) Å and 2.609(4) Å] and is *trans* to the longest titanium−chlorine bond [2.371(4) Å compared to 2.331(4) Å and 2.358(3) Å]. There is no evidence of any agostic interactions in the solid-state structure or in the infrared spectrum.

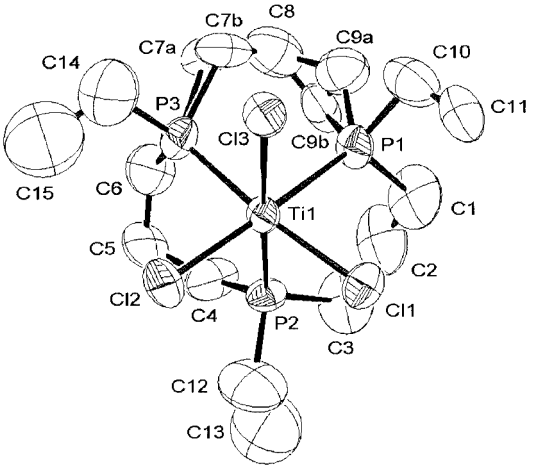


Figure 1. A view of the X-ray crystal structure and atom labelling scheme of ([12]ane$P_3Et_3$)$TiCl_3$ (**1**); thermal ellipsoids are set at 50% probability

There are a few examples of tris(monophosphane)titanium(III) complexes. $TiCl_3P_3$ (P = $PCy_3$, P*i*$Pr_3$, $PBu_3$) which have been reported to form at low temperatures, but at higher temperatures phosphane dissociation occurs and $TiCl_3P_2$ predominates.[5,6] The tridentate ligand trimpsi {trimpsi = *tert*-butyltris[(dimethylphosphanyl)methyl]silane, *t*BuSi($CH_2PMe_2$)$_3$} forms a complex with $TiCl_3$ but the crystal structure has not been reported.[8] All crystallographically characterised (phosphane)$Ti^{III}$ complexes contain cyclopentadienyl ligands except $Ti(BH_4)_3(PMe_3)_2$ which shows M−P distances of 2.571(3) and 2.539(3) Å;[9] All known titanium−phosphane distances fall within the range 2.58±0.07 Å, regardless of oxidation state or coordination number. The P−Ti−P bond angles in **1** are somewhat compressed [average 82.71(13)°] compared to those of **2** and **3** although they are similar to those reported for (trimpsi)$Ti(CO)_4$, and other chelating phosphanes more generally.[8]

The addition of [12]ane$P_3Et_3$ to $VCl_3$·3THF gives rise to ([12]ane$P_3Et_3$)$VCl_3$ (**2**) which may be isolated as a green crystalline solid in good yield. Analytical and mass spectrometric data confirm the nature of **2** and the magnetic susceptibility is consistent with $d^2$ $V^{III}$. Somewhat surprisingly, this complex is almost indefinitely stable to air as a solid, but it is moderately air-sensitive in solution. There are numerous other (phosphane)$V^{III}$ complexes known but these contain mainly monodentate phosphanes and are stabilised by cyclopentadienyl ligands;[10] notable exceptions are [$(Me_2PCH_2CH_2)_2N$]$VCl_2$ (and organometallic derivatives)[11] and (trimpsi)$VCl_3$,[7] although neither have been structurally characterised. The crystal structure of **2** is shown in Figure 2, selected bond lengths and angles are given in Table 1. There are no related structurally characterised six-coordinate (phosphane)vanadium(III) complexes with which to make comparisons (five-coordination being more common for simple $V^{III}$ complexes); however, the vanadium−phosphane bond lengths in **2** are similar to

Table 1. Selected bond lengths [Å] and angles [°] for compounds **1**−**6**

| | **1** | **2** | **3** | **4** | **5** | **6** |
|---|---|---|---|---|---|---|
| M−P | 2.608(4) | 2.514(3) | 2.444(2) | 2.408(10) | 2.465(2) | 2.526(3) |
| | 2.609(4) | 2.519(3) | 2.447(2) | 2.451(9) | 2.443(2) | 2.528(3) |
| | 2.623(4) | 2.526(3) | 2.450(2) | 2.596(10) | 2.431(2) | 2.511(3) |
| M−Cl | 2.331(4) | 2.324(3) | 2.328(2) | 2.365(10) | 2.345(2) | 2.323(3) |
| | 2.358(3) | 2.325(3) | 2.333(2) | 2.295(10) | 2.328(2) | 2.324(3) |
| | 2.371(4) | 2.347(3) | 2.351(2) | | 2.331(2) | 2.302(3) |
| M=O | – | – | – | 1.836(18) | – | – |
| P−M−P | 81.58(12) | 88.83(11) | 90.72(8) | 89.8(3) | 89.41(8) | 87.77(9) |
| | 81.18(13) | 87.22(10) | 90.83(7) | 81.9(3) | 91.05(7) | 87.46(10) |
| | 85.38(13) | 86.40(10) | 91.52(8) | 82.5(3) | 91.02(7) | 89.74(10) |
| Cl−M−Cl | 100.77(14) | 102.12(12) | 98.07(8) | 95.0(3) | 95.84(8) | 97.64(10) |
| | 101.41(14) | 95.54(12) | 96.80(8) | | 97.47(7) | 94.64(10) |
| | 100.41(14) | 100.85(11) | 97.01(8) | | 97.51(7) | 104.99(10) |
| P−V−O | – | – | – | 92.0(6) | – | – |
| | | | | 91.9(6) | | |
| | | | | 171.7(5) | | |
| Cl−V−O | – | – | – | 98.7(6) | – | – |
| | | | | 100.3(6) | | |

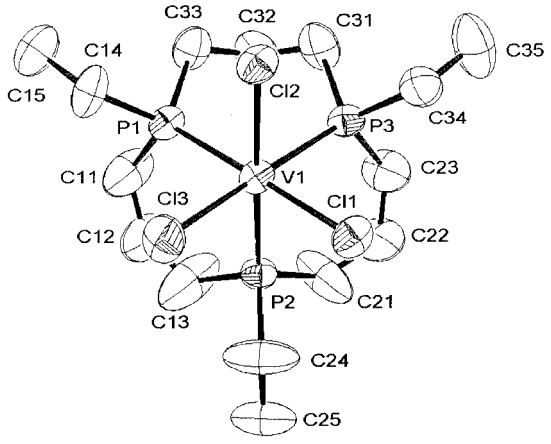


Figure 2. A view of the X-ray crystal structure and atom labelling scheme of ([12]ane$P_3Et_3$)$VCl_3$ (**2**); thermal ellipsoids are set at 50% probability

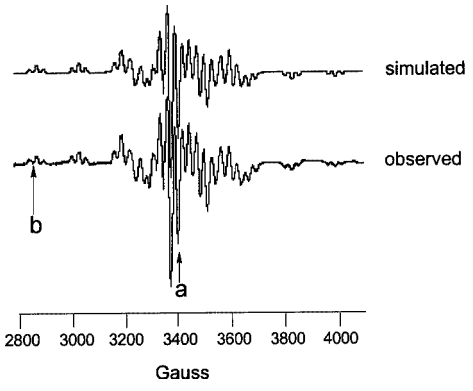


Figure 3. X-band EPR spectrum of **4** recorded in $CD_2Cl_2$/[$D_8$]toluene at 10 K

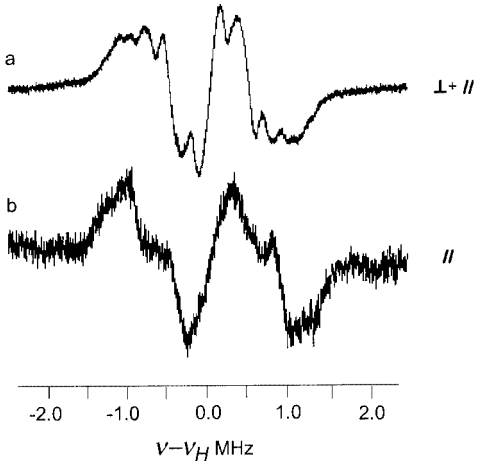


Figure 4. $^1$H ENDOR spectrum of **4** measured at 10 K; spectrum (a) was recorded at the field position a, and spectrum (b) recorded at field position b, shown in Figure 3

those reported for $VCl_3(PMePh_2)_2$ [av. 2.527(18) Å][12] and $CpVCl_2(PMe_3)_2$ [av. 2.509(1) Å].[13] Although there is no significant difference in the V−P distances between **2** and complexes of monodentate phosphanes, the five-coordinate complexes are coordinatively unsaturated which presumably contributes to their much greater sensitivity to air and moisture. The preferential oxidation of the metal in **2** also suggests that the M−P bond is relatively inert. The majority of monodentate phosphane complexes are labile in solution (as shown by the ease in which they can be replaced with alternative σ-donor ligands), but the macrocyclic coordination effect, coupled with the coordinative saturation appears to make **2** more stable than (phosphane)vanadium complexes previously reported.

The EPR spectrum of **2** does not show a resonance due to the $d^2$ $V^{III}$ centre. The absence of an observable EPR signal could also be due to relaxation effects which are not quenched even at low temperatures (10 K). Indeed, there are very few examples of EPR-active $V^{III}$ species.[14] Exposure of solutions of **2** to air results in EPR and ENDOR spectra (Figures 3 and 4, respectively, corresponding spin Hamiltonian parameters are listed in Table 2) which can be assigned to the oxidation product of **2**, ([12]ane$P_3Et_3$)-$V(O)Cl_2$ (**4**). This EPR spectrum displays a characteristic superhyperfine pattern composed of a triplet of doublets, superimposed on the $^{51}$V hyperfine lines (most clearly seen in the outer $m_I = \pm 7/2, \pm 5/2$ lines of the $A_{\|}$ component). As discussed in detail below, this superhyperfine pattern demonstrates the presence of two distinct phosphorus environments in **4**. Compound **4** can also be prepared and isolated in high yield by bubbling air through a dichloromethane solution of **2** containing a few drops of water. It is interesting to note that phosphane oxide is not formed by this procedure, again illustrating the relative robustness of these macrocyclic phosphane complexes. In addition to the molecular ion for **4** being observed in the mass spectrum, analytical data is consistent with the formulation and magnetic susceptibility confirms the presence of $d^1$ $V^{IV}$.

Table 2. Spin Hamiltonian parameters for **1**, **4**, and **7**

| Complex | Nucleus | $g_{\|}$ | $g_{\perp}$ | $A_{\|}$ [G] | $A_{\perp}$ [G] |
|---|---|---|---|---|---|
| **1** | $^{48}$Ti × 1 | 1.9695 | 1.915 | – | – |
| | $^{31}$P × 2 | – | – | 19.1 | 21 |
| | $^{31}$P × 1 | – | – | unres. | unres. |
| | $^{35,37}$Cl × 2 | – | – | unres. | unres. |
| **4** | $^{51}$V × 1 | 1.978 | 1.984 | 153 | 50 |
| | $^{31}$P × 2 | – | – | 24.5 | 27 |
| | $^{31}$P × 1 | – | – | 6 | 6.1 |
| | $^{35,37}$Cl × 2 | – | – | 0.1 | 3 |
| **7** | $^{92}$Nb × 1 | 1.958 | 1.965 | 222 | 115 |
| | $^{31}$P × 2 | – | – | 28 | 26 |

The deep blue, air-stable **4** has been structurally characterised and its crystal structure is shown in Figure 5, with selected bond lengths and angles shown in Table 1. This is the first reported complex to have an octahedral VO unit with phosphanes as ligands; the only other vanadyl species with ancillary phosphane ligands are $V(O)Cl_2(PPh_3)_2$

(which shows a trigonal-bipyramidal structure with the phosphane ligands in the axial positions[15]) and $V(O)Cl_2[P(SiMe_3)_3]_2$ [16] (which shows the same structural motif). Compound **4** can be described as a distorted octahedral complex with an unusually long V=O bond of 1.836(18) Å, and this is manifested in the infrared spectrum which shows a low-frequency V=O stretch at 936 $cm^{-1}$. The majority of vanadyl complexes are five-coordinate with a relatively short V=O bond (typically 1.55−1.68 Å) which is often considered to have some triple-bond character. For example $VOCl_2(NMe_3)_2$[17] has a V=O bond length of 1.590(2) Å, whilst in $V(O)Cl_2[P(SiMe_3)_3]_2$ the V=O bond length is 1.602 Å although the $V(O)Cl_2$ unit is disordered. The bond lengths in **4** show that there are two significantly different phosphorus environments (also indicated in the EPR spectrum); the V−P bond *trans* to the oxo group is longer than that to the equatorial phosphane moieties by 0.14(3) Å. Differences in V−P distances are substantially greater than those which may be attributed to Jahn−Teller distortions in **1** and **2**; this is presumably due to the high *trans* influence of the oxygen atom which commonly dictates the predominance of five-coordination in vanadyl chemistry. The relatively weak V=O bond can, in turn also be explained by a *trans* influence of the σ-donor phosphane ligand. This structure is a unique example of a V=O unit with a phosphane ligand in *trans* position and demonstrates the significance of the *trans* influence of a phosphane ligand on a bond that is commonly very strong. Recently, a structure of the first example of an imido ligand *trans* to a phosphane ligand has been reported[18] which also shows an unusually long V−P bond *trans* to the imido functionality [V−P = 2.642(2) Å]. The V−P bond length in $V(O)Cl_2(PPh_3)_2$ is 2.6217(11) Å, but this long bond length was ascribed to steric effects of the ligand. The collective shortening of the M−P bonds (in comparison to **2**) on oxidation to a more electropositive +4 state reflects the expected decrease in ionic radius upon oxidation. This feature may also indicate that the phosphane ligand is predominantly acting as a σ-donor, and back donation to the phosphane π-acceptor orbitals is of less importance.

The deep blue chromium complex ([12]ane$P_3Et_3$)$CrCl_3$ (**3**) is an intermediate in the liberation of free [12]ane$P_3Et_3$. The halogen oxidation of the tertiary phosphane macrocycle on a $Cr^0$ template differs to that of the molybdenum complex reported previously. Addition of chlorine to a solution of ([12]ane$P_3Et_3$)$Cr(CO)_3$ yields the chromium(III) complex ([12]ane$P_3Et_3$)$CrCl_3$, whereas under the same conditions, the molybdenum template yields seven-coordinate ([12]ane$P_3Et_3$)$Mo(CO)_2Cl_2$. In contrast, the secondary phosphane macrocycle complex ([12]ane$P_3H_3$)$Cr(CO)_3$ forms an octahedral dicarbonyl(halo)$Cr^{II}$ halide complex.[4] Presumably the greater σ-donor ability of the tertiary phosphane macrocycle is more able to stabilise the higher oxidation state in **3**. Similar halogen oxidations of tricarbonyl$Cr^0$ complexes of linear triphosphanes have been reported to result in oxidation of the metal atom with loss of all carbonyl ligands but also with concomitant oxidation of the phosphane ligand.[18] Compound **3** can also be synthesised

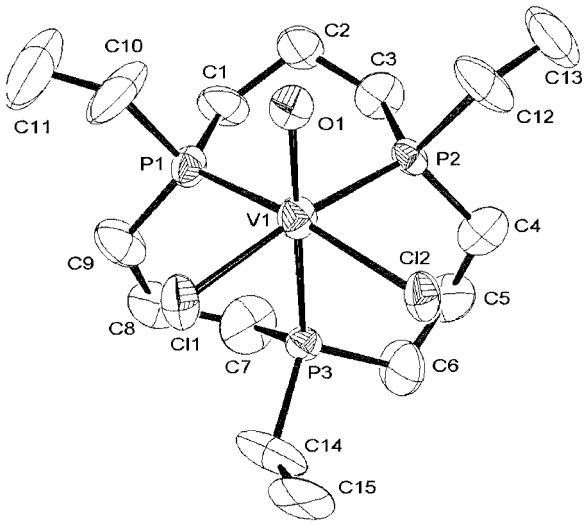


Figure 5. A view of the X-ray crystal structure and atom labelling scheme of ([12]ane$P_3Et_3$)$V(O)Cl_2$ (**4**); thermal ellipsoids are set at 50% probability

by the addition of [12]ane$P_3Et_3$ to a suspension of $CrCl_3(THF)_3$; crystals isolated by either method give rise to satisfactory analytical, mass spectrometric and magnetic susceptibility data.

The crystal structure of **3** is shown in Figure 6 and selected bond lengths and angles are shown in Table 1. The structure shows the macrocycle facially capping an octahedral metal atom, as expected. The average Cr−P bond length is 2.447(3) Å, whilst the average Cr−Cl bond length is 2.337(2) Å and variations in these distances are less than for **1** and **2** as might be expected for a $d^3$ metal centre. They are also similar to those reported for *fac*-[$CrCl_3$(tripod)] [Cr−P 2.456(2) Å (av.); Cr−Cl 2.306(2) Å (av.)] [tripod = $MeC(CH_2PMe_2)_3$][19] and *mer*-[$CrCl_3\{P(CH_2CH_2PPh_2)_3\}$] [av. Cr−P and Cr−Cl are 2.451(5) and 2.306(5) Å, respectively].[20] The average P−Cr−P angles in **3** [91.02(8)°] are close to the ideal values for an octahedron, unlike those in *fac*-[$CrCl_3$(tripod)] [83.47(7)°]. This difference indicates a greater flexibility in the macrocycle compared to the tripodal phosphane; restricted flexibility in tripodal ligands of this type has previously been commented on.[19]

Addition of [12]ane$P_3R_3$ to solutions of $TiCl_4$, $ZrCl_4$, and $HfCl_4$ resulted in coordination of the macrocycle (verified by $^{31}P$ NMR spectroscopy) although tractable materials could not be isolated. In the case of Zr and Hf, singlets with relatively small coordination chemical shifts were observed ($\Delta\delta$ = 15, 16 ppm, respectively) which showed only a small and linear temperature dependence and remained unchanged upon addition of excess ligand (indicating the absence of facile ligand exchange processes).

### $M^{III}$ Complexes of Pendant Ether Macrocycles

We have previously reported the synthesis of a series of ([12]ane$P_3R_3$)$M(CO)_3$ complexes (M = Mo, Cr; R = alkyl chain with a pendant donor function).[21] Oxidation of these chromium compounds with chlorine gives rise to ([12]ane$P_3R_3$)$CrCl_3$ (R = $H_3COC_3H_6$, $C_2H_5OC_2H_4$) in

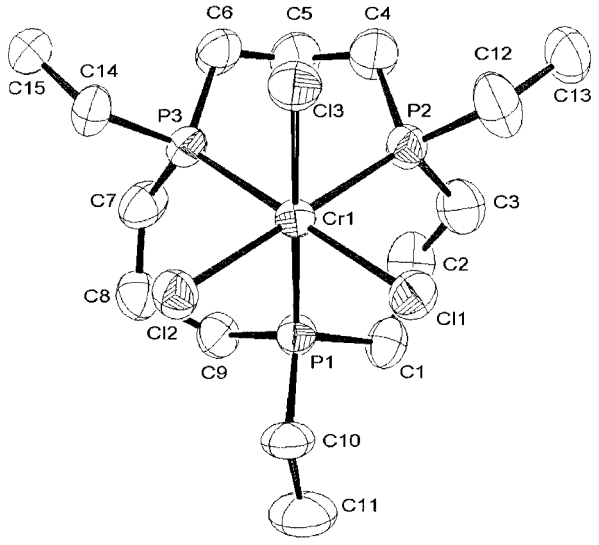


Figure 6. A view of the X-ray crystal structure and atom labelling scheme of one of the two independent molecules of ([12]ane$P_3$-$Et_3$)$CrCl_3$ (**3**); thermal ellipsoids are set at 50% probability; pyridine of crystallisation is omitted for clarity

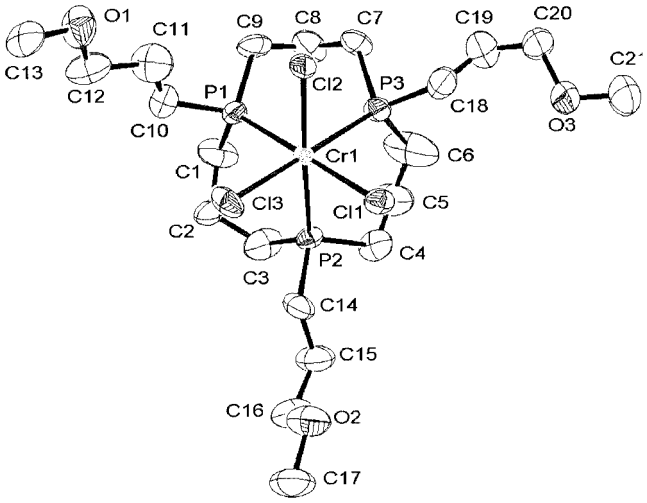


Figure 7. A view of the X-ray crystal structure and atom labelling scheme of {[12]ane$P_3$($C_3H_6OMe)_3$}$CrCl_3$ (**5**); thermal ellipsoids are set at 50% probability

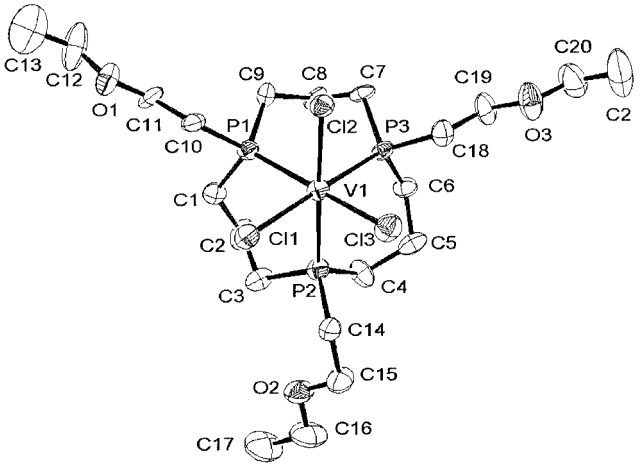


Figure 8. A view of the X-ray crystal structure and atom labelling scheme of {[12]ane$P_3$($C_2H_4OEt)_3$}$VCl_3$ (**6**); thermal ellipsoids are set at 50% probability

good yield. The crystal structure of [1,5,9-tris(3-methoxypropyl)-1,5,9-triphosphacyclododecane]chromium trichloride (**5**) is shown in Figure 7 and selected bond lengths and angles are given in Table 1. The structure (bond lengths and angles) is very similar to that of **3** which is not unexpected. Liberation of the macrocycle by digestion in strong base gives rise to the free macrocycle stereospecifically and in good yields. Reaction of the ethoxyethyl pendant donor macrocycle with $VCl_3(THF)_3$ gives rise to the green solid **6** that is similar to **2**. The crystal structure is shown in Figure 8 and selected bond lengths and angles are given in Table 1. The vanadium atom is facially capped by the macrocycle and the pendant donor atoms are well away from the metal centre, indicating that there is no bonding interaction in the solid state. The structural features are very similar to those of **2**. Attempts to force coordination of at least one pendant arm by halide abstraction have so far proved unsuccessful.

### $Nb^{III}$ and $Nb^{IV}$ Complexes

The addition of 1 mol-equiv. of [12]ane$P_3Et_3$ to a frozen solution of $NbCl_3$(DME) or $NbCl_4(THF)_2$ in dichloromethane followed by warming gives rise to paramagnetic, air-sensitive solutions, manipulation of these caused decomposition (to oily materials) precluding the measurement of reliable characterisation data although EPR spectroscopy of these solutions confirmed the presence of $d^2$ $Nb^{III}$ and $d^1$ $Nb^{IV}$, respectively. The $Nb^{IV}$-containing solution is reversibly thermochromic, being deep blue at ca. −30 °C and green at ambient temperature (20 °C). These colours are precedented for chloro(phosphane)niobium complexes and could be due to a temperature-dependent monomer/dimer equilibrium since $NbCl_4(dmpe)_2$ is blue[22] whilst $Nb_2Cl_8(PMe_3)_4$ is green.[23] The behaviour of the $Nb^{III}$-containing solutions is similar to those of **4** in that brief exposure to air gives rise to the loss of a resonance attributable to $Nb^{III}$ and the appearance of a new EPR spectrum that can be attributed to the $d^1$ $Nb^{IV}$ species **7** (vide infra). Attempts to grow crystals of these Nb compounds failed. Addition of [12]ane$P_3Et_3$ to $Nb(O)Cl_3(MeCN)_2$ gave rise to an intractable white precipitate which was not further characterised.

### EPR and ENDOR Spectroscopy

The EPR spectra of **1** and **4** are shown in Figures 9 and 3, respectively. The spin Hamiltonian parameters for the $Ti^{3+}$ and $V^{4+}$ complexes were obtained by computer simulations (Figures 10 and 3, respectively) and the values used are presented in Table 2. Both systems are characterised by an axial $g$ tensor of the form $g_{\|} > g_{\perp}$ which indicates that the metal ion experiences a tetragonally distorted octahedral environment. The high abundance of $^{51}V$ ($I$ = 7/2) dominates the spectrum of **4**. The $Ti^{3+}$ and $V^{4+}$ ions have sim-

ilar $d^1$ electronic structures, and based on the similarities with the $g$ values ($g_\perp = 1.915$ for Ti and 1.984 for V; $g_\parallel = 1.9695$ for Ti and 1.978 for V) both spectra are consistent with a similar crystal-field environment. Therefore, although the EPR spectra appear different, they imply very similar structures and confirm the tetragonal distortion in both **1** and **4**.

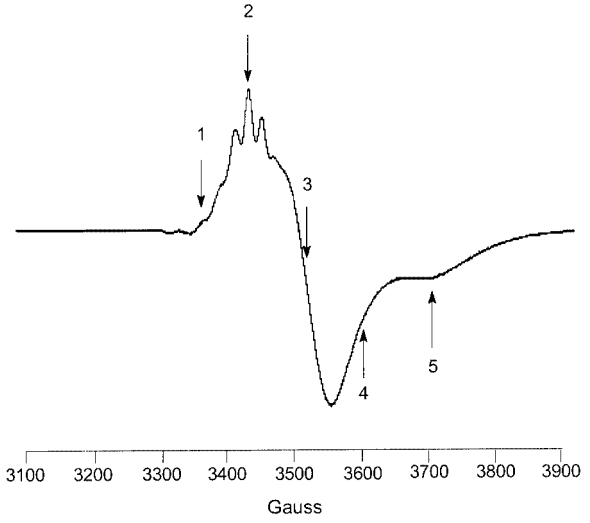


Figure 9. X-band EPR spectrum of **1** recorded in $CD_2Cl_2$/[$D_8$]toluene at 10 K

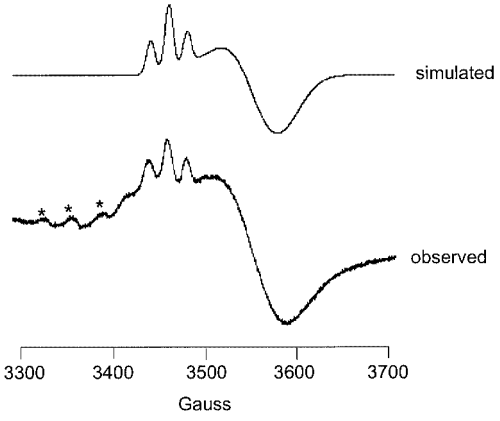


Figure 10. Computer simulation of the X-band EPR spectrum of **1**; the peaks marked * in the experimental spectrum are due to artefacts caused by the inhomogeneous nature of the sample or impurities in the complex

Due to the unpaired $d^1$ electron not being completely delocalised in the metal d orbitals, a weak superhyperfine interaction with the surrounding ligands can be observed; this is most clearly evident in the vanadyl spectrum (Figure 3). The outer $^{51}V$ hyperfine lines in Figure 3 clearly reveal a pattern composed of a triplet of doublets and this originates from the weak coupling between the $d^1$ electron and two equivalent phosphane moieties, and a smaller coupling to a third phosphorus nucleus. The two equivalent phosphane moities produce the triplet pattern while the third remote phosphorus nucleus creates the smaller doublet structure. Thus, the unpaired spin of the $V^{4+}$ ion is delocalised onto the surrounding phosphorus nuclei, two of which are equivalent while the third is slightly more distant, a structural feature also observed in the crystalline state by X-ray crystallography. This EPR spectrum looks remarkably similar to that reported for $VOCl_2(PEt_3)_2$, except for the presence of the weak coupling to the third phosphorus atom, whilst the $g$ and $A$ values are almost identical.[13] The EPR spectrum of **4** was sufficiently resolved, that accurate values of the $^{31}P$ superhyperfine tensors could be obtained. The values of $^{P}A_\parallel = 24.5$ G, $^{P}A_\perp = 27$ G for the two equivalent phosphane moities and $^{P}A_\parallel = 6$ G, $^{P}A_\perp = 6.1$ G for the third inequivalent P nucleus, were tested by computer simulation (Figure 3). It was necessary to introduce a small contribution from two equivalent Cl nuclei in order to improve the quality of the fit. The satisfactory fit between the experimental and simulated spectra confirm the accuracy of the assignments (Table 2). These superhyperfine couplings were subsequently used to estimate the extent of electron delocalisation onto the P nuclei, and the results of this analysis are given in Table 3.

Based on the spin Hamiltonian parameters used in the simulations, we can suggest that the two chlorine nuclei are virtually equivalent and therefore approximately equidistant from the V centre. The s and p orbital spin density on the Cl nuclei is also found to be appreciably larger compared to the P nuclei (Table 3). This indicates, to a first approximation, that the V−Cl distances are slightly shorter compared to the V−P distances (as demonstrated from the crystal structures) and thereby produce a larger superhyperfine interaction. Although the spin densities are higher on $^{35}Cl$, the $A_O$ and $B_O$ values for $^{31}P$ are larger than $^{35}Cl$, so that a larger $^{31}P$ splitting is observed in the spectrum.

The EPR spectrum for the $Ti^{3+}$ complex **1** was less well resolved and the lines significantly broader, so only the larger superhyperfine interaction with the phosphorus nuclei could be simulated with any degree of accuracy (seen as a triplet in the $g_\parallel$ region i.e. position 2 in Figure 9). The spin Hamiltonian parameters used in the simulations are given in Table 2. As for the vanadium case discussed above, two of the phosphane nuclei appear to be equivalent, while the third one was not resolved, presumably in part due to a relatively small superhyperfine coupling consistent with a tetragonally distorted structure. Again this feature is also confirmed by X-ray crystallography.

Electron nuclear double resonance (ENDOR) measurements were also made on **1** and **4** and the results are shown in Figures 11 and 4, respectively. Although the EPR spectrum of **4** was well resolved, it was not sufficiently intense to allow detailed ENDOR measurements to be made. The $^1H$ ENDOR spectra, measured at the field positions marked a and b in Figure 3, are shown in Figure 4. However, the titanium EPR spectrum (1), was sufficiently intense that a detailed magnetic angle selected ENDOR analysis could be performed as shown in Figure 11.

The ENDOR spectra of **1** and **4** (Figures 11 and 4, respectively) were recorded at positions corresponding to the $z$ axis of the EPR framework (i.e. in **4** this is the V=O bond direction), while the perpendicular direction refers to the $xy$

Table 3. Calculated spin densities on surrounding nuclei for **1**, **4**, and **7**

| Complex | Nucleus | $A_O$ [G] | $B_O$ [G] | $a_{iso}$ [G] | $B$ [G] | $C_S^2$ | $C_P^2$ | Spin density |
|---|---|---|---|---|---|---|---|---|
| **1** | $^{31}P \times 2$ | 3631 | 102 | 20.3 | 0.633 | 0.559% | 0.62% | 1.18% |
| **4** | $^{31}P \times 2$ | 3631 | 102 | 26.1 | 0.833 | 0.72% | 0.816% | 1.53% |
| | $^{31}P \times 1$ | 3631 | 102 | 6.0 | 0.05 | 0.16% | 0.05% | 0.21% |
| | $^{35,37}Cl \times 2$ | 1665 | 48.6 | 2.03 | 0.966 | 0.12% | 1.98 | 2.1% |
| **7** | $^{31}P \times 2$ | 3631 | 102 | 26.6 | 1.66 | 0.72% | 1.62% | 2.024% |

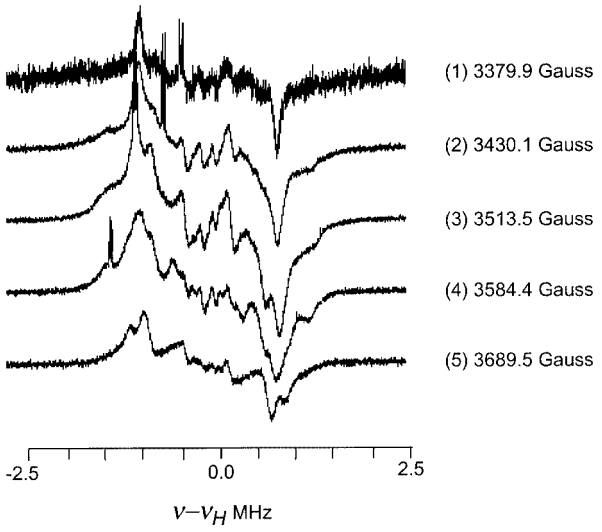


Figure 11. $^1H$ ENDOR spectra of **1** recorded at 10 K in $CD_2Cl_2$/[$D_8$]toluene; the spectra marked (1)−(5) were recorded using the static field positions of 3379.9 G (1), 3430.1 G (2), 3513.5 G (3), 3584.4 G (4), 3689.5 G (5), as shown in Figure 9

plane. In both ENDOR spectra, strong couplings (of approx. 1 MHz) and smaller, more poorly resolved inner couplings of less than 0.5 MHz are observed. It is interesting to note that the ENDOR spectra are slightly different for both samples. In the vanadium case a strong peak is clearly visible with a coupling of about 1 MHz but a distinctive shoulder at about 1.3 MHz, can also be seen (Figure 4, b). Based on the structures of the two complexes, two dominant groups of protons are expected, corresponding to the protons of the cyclododecane ring and those of the ethyl groups. The former set of protons are closer to the V nucleus and would therefore be expected to produce the larger ENDOR coupling compared to the more remote ethyl groups. It may therefore be suggested that the strong coupling of ca. 1 MHz corresponds to the cyclododecane protons while the inner and less well-resolved couplings of ca. 0.5 MHz are due to the ethyl groups. The differences between the titanium and vanadium $^1H$ ENDOR spectra are very small, however, and the implied inequivalency of the $CH_2$ protons cannot be confirmed by alternative spectroscopic methods (e.g. by IR spectroscopy). The ENDOR spectrum measured at position 2 in Figure 9 refers to a position in which the magnetic field is pointing "off-axis", between the $z$ direction and the $xy$ plane. In this case, the ENDOR spectrum becomes much more complicated as several molecular orientations are selected simultaneously, and very careful simulation is needed in order to assign each coupling to a specific $CH_2$ group.

The EPR spectrum of **7** (Figure 12) is strikingly similar to that of ([12]ane$P_3Et_3$)V(O)$Cl_2$ (**4**). The shape of the spectrum and the spin Hamiltonian parameters reveal that the symmetry and electronic configuration of the metal atoms must be analogous in both cases, i.e. it indicates that the overall structural features are very similar to those of ([12]ane$P_3Et_3$)V(O)$Cl_2$. The presence of two equivalent phosphane moieties is again demonstrated by the characteristic triplet pattern discussed above for **4** (Table 2), but unfortunately the slightly more distant phosphane group cannot be simulated with any degree of accuracy due to the larger EPR linewidths. The $g$ values for the vanadyl and niobyl complexes (Table 2) are both axial in nature, and the average $g$ values for the niobyl complex are slightly lower, which is expected considering the larger spin-orbit coupling constant for Nb compared to V. The similar shifts in $g$ values ($\Delta g = 0.006$ for V and $\Delta g = 0.007$ for Nb), however, indicates similar symmetries for both ions. These values also suggest that the unpaired electron is either in the $d_{xy}$ or $d_{x^2-y^2}$ orbital.

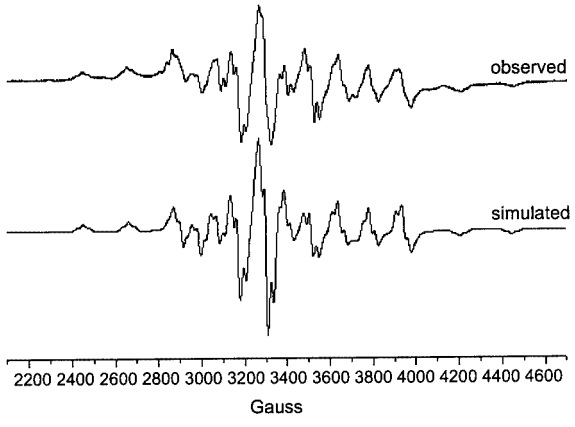


Figure 12. X-band EPR spectrum of **7** recorded in $CD_2Cl_2$/[$D_8$]toluene at 10 K

The superhyperfine interaction of the Nb nucleus with the $^{31}P$ nuclei can be analysed in order to extract some spatial information on the M−P (M = V, Nb) distances. This can be done by breaking the hyperfine tensor into an isotropic ($a_{iso}$) and anisotropic ($B$) component. The anisotropy is very small compared to the isotropic coupling and it can be accounted for on the basis of dipolar interactions

through space between the unpaired electron and the phosphorus nuclei. This assumption is reasonable as little backbonding is expected with the $d^1$ metal ions.

A simple point dipole model can be used to calculate the contribution to the anisotropic coupling from dipolar sources. With this approximation, the distance between the metal centre (V and Nb) and the interacting phosphane nucleus can be determined. Using this model and a calculated anisotropic term of 1.32 G (3.6174 MHz) and 1.66 G (4.5956 MHz) for the vanadyl and niobyl compounds, respectively, the estimated distances are calculated as V−P = 2.388 Å and Nb−P = 2.587 Å. The shortest experimentally determined V−P bond length is 2.408(10) Å (from the crystal structure of **4**), which is in good agreement with the calculated bond length based on the EPR data. The resolution of the third inequivalent P nucleus was not sufficiently good to allow an accurate estimation of the V−P bond length for this more remote phosphane group. On the basis of the EPR spectrum, its satisfactory simulation and the metrical parameters obtained, we tentatively assign the formula ([12]ane$P_3Et_3$)Nb(O)$Cl_2$ to **7**. Although incompletely characterised, **7** is only the second example of an oxo(phosphane)niobium(IV) complex, the first being Nb(O)$Cl_2(PEt_3)_2$.[24] Crystals of **7** were not obtained, and there are only three crystallographically characterised examples of phosphane complexes containing Nb=O, these being compounds of $d^0$ $Nb^V$. Nevertheless, the M−P bond length is 2.64(3) Å in Nb(O)$Cl_3(PMe_3)_3$,[25] and 2.708 Å in [$Et_3$PH][Nb(O)$Cl_4(PEt_3)$],[15] which compare well with the calculated bond length in **7** from the EPR data.

## Conclusion

We have demonstrated that the ligand [12]ane$P_3Et_3$ forms relatively robust six-coordinate complexes with early transition metals. We have reported the structural characterisation of a range of complexes and shown that the EPR and ENDOR spectra of these compounds are highly informative and not only confirm the structural features determined by crystallography but also give substantial insight into the nature of paramagnetic niobium species for which other reproducible data could not be obtained. The first complex with a phosphane ligand *trans* to an oxo function in $V^{IV}$ has been reported and the ligand effect on the V=O bond has been investigated. Preliminary results indicate that the complexes described are reactive towards alkylating agents, other metathetical reagents and are active in alkene polymerisation catalysis; details of these studies will be published in due course. The results also imply that the macrocycle coordination effect helps stabilise these phosphane complexes in relatively regular six-coordinate environments, whereas for higher coordination numbers, this effect is not as substantial as expected and tractable seven-coordinate $d^0$ $M^{IV}$ complexes could not be obtained. This might result from the flexibility of the 12-membered macrocycle as well as stereochemically nonrigid (and intrinsically more reactive) seven-coordination. Consequently, smaller ring macrocycles might be expected to form more stable systems and the study of 9-,[26,27] 10-,[28] and 11-membered triphosphorus macrocycles is in progress.

## Experimental Section

All reactions were carried out under nitrogen (purified by passing through a CrO column) using standard Schlenk line techniques or in a Vacuum Atmospheres drybox. Solvents were dried with standard drying agents and distilled immediately before use. Petroleum ether had a boiling range of 40−60 °C. The Zr, Hf, and Nb halides were sublimed before use. All other chemicals were dried over molecular sieves (liquids) or used as received (Aldrich). The compounds $TiCl_4(THF)_2$, $ZrCl_4(THF)_2$, $HfCl_4(THF)_2$, $TiCl_3(THF)_3$, $VCl_3(THF)_3$,[29] $NbCl_4(THF)_2$, $NbCl_3$(DME),[30] Nb(O)$Cl_3$(MeCN)$_2$,[26] [12]ane$P_3Et_3$,[4] [12]ane$P_3Et_3Cr(CO)_3$, and ([12]ane$P_3R_3$)$Cr(CO)_3$ (R = $CH_3OC_3H_6$. $C_2H_5OC_2H_4$)[22] were prepared by literature methods. $^1H$ and $^{13}C$ NMR spectra were recorded with a Bruker DPX400 spectrometer operating at 400.13 MHz and 100 MHz, respectively. $^{31}P$ NMR spectra were acquired using a JEOL FX90Q at 36.2 MHz and referenced to 85% $H_3PO_4$. Magnetic moments were determined by the Evans method[31] or by the Gouy method with a Johnson Matthey magnetic susceptibility balance; an experimental diamagnetic correction was measured for the free phosphane macrocycles and applied. Mass spectra (EI) were recorded with a VG Platform II Fisons mass spectrometer. Infrared spectra were recorded with a Nicolet 510 FT-IR spectrometer as a nujol mull between CsI plates. The EPR/ENDOR spectra were recorded with a CW X-band Bruker ESP 300E series spectrometer equipped with an ESP360 DICE ENDOR unit, operating at 12.5 kHz field modulation in a Bruker EN 801 cavity. All spectra (EPR and ENDOR) were recorded at 10 K using an Oxford instruments ESR 900 continuous flow He Cryostat; the ENDOR spectra were obtained at 4 mW microwave power, 8 dB RF power from a ENI A-300 RF amplifier again at 12.5 kHz modulation frequency. Computer simulations were carried out using Bruker's Simfonia program.

**([12]ane$P_3Et_3$)$TiCl_3$ (1):** To a purple solution of $TiCl_3(THF)_3$ (0.20 g, 0.51 mmol) in dichloromethane (20 mL) was added a solution of [12]ane$P_3Et_3$ (0.15 g, 0.51 mmol) in dichloromethane (10 mL). The solution immediately turned blue and a fine grey precipitate was observed. This was stirred for 2 h, filtered and the solvent removed in vacuo. The blue residue was washed with petroleum ether (3 × 10 mL) and recrystallised from dichloromethane/petroleum ether at −30 °C to give (0.21 g, 90%) of **1**. Crystals suitable for X-ray analysis were obtained by vapour diffusion of petroleum ether into a dichloromethane solution. $C_{15}H_{33}Cl_3P_3Ti$ (460.6): calcd. C 39.09, H 7.17; found: C 38.7, H 7.0. IR (nujol): $\tilde{\nu}_{max}$ = 1377 (sh), 1072 (br), 802 (br), 376 (br), 257 (w), 210 (w) $cm^{-1}$. MS: $m/z$ = 460.57 [$M^+$]. $\mu_{eff}$ = 1.82 BM.

**([12]ane$P_3Et_3$)$VCl_3$ (2):** To a red solution of $VCl_3(THF)_3$ (0.20 g, 0.50 mmol) in dichloromethane (20 mL) was added a solution of [12]ane$P_3Et_3$ (0.15 g, 0.50 mmol) in dichloromethane (10 mL). The solution immediately turned green and a light green precipitate was observed. This was stirred for 2 h, filtered, and the solvent removed in vacuo. The green residue was washed with petroleum ether (3 × 10 mL) and recrystallised from dichloromethane/petroleum ether at −30 °C to give **2** (0.22 g, 94%). Crystals suitable for X-ray analysis were obtained by vapour diffusion of petroleum ether into a dichloromethane solution. $C_{15}H_{33}Cl_3P_3V$ (463.6): calcd. C 38.67, H 7.52; found: C 38.4, H 7.5. IR (nujol): $\tilde{\nu}_{max}$ = 1269 (sh), 1121

Table 4. Crystallographic data for **1**−**6**; * pent = pentane of solvation, py = pyridine of solvation

| | **1** | **2**·1/2(pent)* | **3**·1/2(py)* | **4** | **5** | **6** |
|---|---|---|---|---|---|---|
| Empirical formula | $C_{15}H_{33}Cl_3P_3Ti$ | $C_{17.5}H_{39}Cl_3P_3V$ | $C_{17.5}H_{35.5}Cl_3CrN_{0.5}P_3$ | $C_{15}H_{33}Cl_2P_3VO$ | $C_{21}H_{43}Cl_3CrO_3P_3$ | $C_{24}H_{52}Cl_3O_3P_3V$ |
| Formula mass | 460.57 | 499.69 | 504.22 | 444.16 | 594.81 | 638.86 |
| Temp. [K] | 150(2) | 150(2) | 293(2) | 150(2) | 150(2) | 293(2) |
| Crystal system | triclinic | monoclinic | monoclinic | triclinic | monoclinic | monoclinic |
| Space group | $P\bar{1}$ | $P2_1/n$ | $P2_1/n$ | $P\bar{1}$ | $P2_1/a$ | $P2_1/n$ |
| $a$ [Å] | 7.774(6) | 9.191(4) | 14.579(3) | 7.577(7) | 17.743(4) | 8.553(1) |
| $b$ [Å] | 9.381(5) | 19.371(3) | 12.268(3) | 8.966(6) | 8.5355(4) | 29.386(2) |
| $c$ [Å] | 15.228(7) | 14.048(1) | 27.424(4) | 15.569(15) | 18.910(2) | 12.683(4) |
| α [°] | 88.320(11) | 90 | 90 | 87.19(5) | 90 | 90 |
| β [°] | 85.020(14) | 102.737(5) | 103.859(13) | 83.70(4) | 102.54(2) | 92.56(1) |
| γ [°] | 80.200(19) | 90 | 90 | 80.80(6) | 90 | 90 |
| $V$ [Å$^3$] | 1090.1(11) | 2439.5(11) | 4762.2(16) | 1037.2(15) | 2795.5(6) | 3184.5(11) |
| $Z$ | 2 | 4 | 8 | 2 | 4 | 4 |
| $D_{calcd.}$ [g/cm$^3$] | 1.403 | 1.361 | 1.407 | 1.422 | 1.413 | 1.332 |
| μ | 0.976 | 0.933 | 1.021 | 0.966 | 0.889 | 0.737 |
| Unique reflections | 2848 | 2186 | 9670 | 1087 | 4217 | 4564 |
| Observed reflections [$I > 2\sigma(I)$] | 1429 | 1449 | 4039 | 485 | | 1181 |
| $R$ (obsd. data) | 0.1042 | 0.0659 | 0.0694 | 0.1012 | | 0.0493 |
| $R_w$ ($wR^2$) (all data) | 0.2598 | 0.1850 | 0.1864 | 0.3061 | | 0.1094 |

(sh), 1072 (sh), 798 (sh), 739 (sh), 491 (br), 385 (w), 341 (br), 278 (w), 239 (w), 217 (w) cm$^{-1}$. NMR ($CD_2Cl_2$): $\delta_H$ = 2.02 (s), −2.82 (s), −3.81 (s), −4.31 (br), −5.05 (s) ppm. MS: $m/z$ = 463.61 [M$^+$], 444.15 [[12]ane$P_3Et_3V(O)Cl_2$]. $\mu_{eff}$ = 2.48 BM.

**([12]ane$P_3Et_3$)$CrCl_3$·0.5py (3). Method 1:** $Cl_2$ was bubbled through a solution of ([12]ane$P_3Et_3$)$Cr(CO)_3$ (2.0 g, 4.5 mmol) in dichloromethane (50 mL) for 5 min. This was stirred for 4 h and the solvent removed in vacuo to yield a violet microcrystalline solid that was recrystallised from dichloromethane to give blue **3** (1.88 g, 90%). Crystals suitable for X-ray analysis were obtained by vapour diffusion of toluene into a pyridine solution of **3**. $C_{17.5}H_{35.5}Cl_3CrN_{0.5}P_3$ (504.3): calcd. C 41.67; H,7.04; found: C 41.7, H 7.2. IR (nujol): $\tilde{\nu}_{max}$ = 310 (br), 240 (w) cm$^{-1}$. $\mu_{eff}$ = 3.66 BM. **Method 2:** To a purple suspension of $CrCl_3(THF)_3$ (0.10 g, 0.25 mmol) in dichloromethane (20 mL) was added a solution of [12]ane$P_3Et_3$ (0.08 g, 0.51 mmol) in dichloromethane (10 mL). The solution immediately turned blue. This was stirred for 4 h, filtered and the solvent removed in vacuo. The blue residue was washed with petroleum ether (3 × 10 mL) and recrystallised from dichloromethane/petroleum ether to give **3** (0.07 g, 65%).

**([12]ane$P_3Et_3$)$V(O)Cl_2$ (4):** To a dichloromethane solution of **2** (0.10 g, 0.22 mmol) was added distilled water (5 mL) and this was stirred for 2 h whilst air was slowly bubbled through the solution. The solution was dried with $CaH_2$, filtered, concentrated to 5 mL and cooled to −30 °C. The resulting blue crystals were isolated and dried in vacuo to yield **7** (0.08 g, 86%). Crystals suitable for X-ray analysis were obtained by slow cooling of a saturated petroleum ether solution. $C_{15}H_{33}Cl_2OP_3V$ (444.2): calcd. C 37.56, H 6.93; found: C 37.0, H 6.2. IR (nujol): $\tilde{\nu}_{max}$ = 936(V=O) cm$^{-1}$. MS: $m/z$ = 444.15 [M$^+$]. $\mu_{eff}$ = 1.65 BM.

**([12]ane$P_3R_3$)$CrCl_3$ (5):** $Cl_2$ was bubbled through a solution of ([12]ane$P_3R_3$)$Cr(CO)_3$ (R = $CH_2CH_2CH_2OCH_3$) (2.0 g, 3.5 mmol) in dichloromethane (50 mL) for 5 min. This was stirred for 4 h and the solvent removed in vacuo to yield a deep blue microcrystalline solid that was recrystallised from dichloromethane/petroleum ether to give **9** (1.79 g, 86%). $C_{24}H_{52}Cl_3CrO_3P_3$ (639.9): calcd. C 42.25, H 7.28; found: C 42.7, H 7.3. IR (nujol): $\tilde{\nu}_{max}$ = 312 (br), 220 (w) cm$^{-1}$. $\mu_{eff}$ = 3.59 BM.

**([12]ane$P_3R_3$)$VCl_3$ (6):** To a red solution of $VCl_3(THF)_3$ (0.20 g, 0.50 mmol) in dichloromethane (20 mL) was added a solution of [12]ane$P_3R_3$ (R = $CH_2CH_2OCH_2CH_3$) (0.22 g, 0.50 mmol) in dichloromethane (10 mL). The solution immediately turned green and a light green precipitate was observed. This was stirred for 2 h, filtered and the solvent removed in vacuo. The green powder was recrystallised from dichloromethane/petroleum ether at −30 °C to give **6** (0.25 g, 84%). Crystals suitable for X-ray analysis were obtained by vapour diffusion of petroleum ether into a dichloromethane solution. $C_{24}H_{52}Cl_3O_3P_3V$ (638.9): calcd. C 45.17, H 8.20; found: C 45.0, H 8.3. IR (nujol): $\tilde{\nu}_{max}$ = 277 (w), 242 (w), 214 (w) cm$^{-1}$. MS: $m/z$ = 638.86 [M$^+$]. $\mu_{eff}$ = 2.51 BM.

**([12]ane$P_3Et_3$)$Nb(O)Cl_2$ (7):** To $NbCl_3$(DME) (0.10 g, 0.34 mmol), frozen in liquid nitrogen, was added a solution of 12[ane]$P_3Et_3$ (0.10 g, 0.34 mmol) in dichloromethane (20 mL) and the mixture allowed to warm to room temperature with gentle agitation. The resulting dark green solution was filtered through Celite. The resulting green solution (in a Schlenk flask) was briefly exposed to air (by removing and replacing the stopper) and the inert gas was immediately reinstated. This solution was transferred to an EPR tube and the spectrum run immediately. Attempts to prepare samples of **7** by addition of water and air (as for compound **4**) resulted in complete decomposition and dissociation of the macrocyclic ligand (by NMR).

**X-ray Crystallography:** The crystal data for compounds **1**−**6** are given in Table 4. For compounds **1**, **2**, **4**−**6**, intensity data were collected with a FAST TV area detector diffractometer at the window of a rotating anode generator, with a molybdenum target [λ(Mo-$K_\alpha$) = 0.71069 Å] and driven by MADNES[32] software (for **2** and **4**). The structures were solved by heavy atom methods (SHELXS)[33] and refined by full-matrix least squares based on $F_o^2$ (SHELXL 93).[34] All non-hydrogen atoms are anisotropic with H-atoms included in calculated positions (riding model) and isotropic displacement parameters which were refined. Diagrams were

drawn with SNOOPI[35] or ORTEP for Windows.[36] Sources of scattering factors are given in ref.[33] For compound **1**, the structure was finally refined to $R = 0.1042$. The quality of the crystal was very poor and it was also a very weak diffractor. One of the three $CH_2CH_2CH_2$ chains was disordered and two of its carbon atoms were refined with partial occupancies. All non-hydrogen atoms were refined anisotropically with ISOR = 0.02 restraints being applied to several carbon atoms. The C−C bond lengths were constrained at 1.52(2) Å. The H atoms of the disordered $CH_2CH_2CH_2$ chain were ignored; all others were included in calculated positions (riding model). For compound **4**, the data were collected with a small and weakly diffracting crystal and refined to a final $R = 0.1012$. The pendant ethyl carbon atoms showed high thermal motion (as is not unexpected for compounds of this nature) and correspondingly large ellipsoids although no positional disorder for these atoms could be satisfactorily modelled. Although the $R$ factors for these two compounds are relatively high, the quality of the structures is adequate to allow comparisons of metal−ligand bond lengths and angles. Data for **3** were obtained with an Enraf−Nonius CAD4 diffractometer. The structure was solved by direct methods and refined on $F^2$ by full-matrix least squares (SHELX97)[37] using all unique data. Empirical absorption corrections were carried out by the DIFABS method.[38] CCDC-171468 (**1**), -143583 (**2**), -171469 (**3**), -143586 (**4**), -171471 (**5**), and -171470 (**6**) contain the supplementary crystallographic data for this paper. These data can be obtained free of charge at www.ccdc.cam.ac.uk/conts/retrieving.html or from the Cambridge Crystallographic Data Centre, 12, Union Road, Cambridge CB2 1EZ, UK [Fax: (internat.) + 44-1223/336-033; E-mail: deposit@ccdc.cam.ac.uk].

## Acknowledgments

We thank Drs. D. Hibbs, S. J. Coles, K. M. A. Malik, T. Albers, and Mr. R. Haigh for assistance with the structural determinations. We also thank the EPSRC for funding (R. J. B and P. C. D), the EPSRC National ENDOR service and the Association of Commonwealth Universities and the University of Sri Jayewardenepura of Sri Lanka for a studentship (S. S. L.).

[1] M. D. Fryzuk, T. S. Haddad, D. J. Berg, *Coord. Chem. Revs.* **1990**, *99*, 137−212.
[2] L. Messerle, *Chem. Revs.* **1988**, *88*, 1229−1254.
[3] *Comprehensive Organometallic Chemistry* (Eds.: E. W. Abel, F. G. A Stone, G. Wilkinson), Pergammon Press, Oxford, UK, **1982**.
[4] P. G. Edwards, J. S. Fleming, S. S. Liyanage, *Inorg. Chem.* **1996**, *35*, 4563−4568.
[5] C. D. Schmulbach, C. H. Kolich, C. C. Hinckley, *Inorg. Chem.* **1972**, *11*, 2841−2843.
[6] N. Koide, K. Iimura, *Polym. Prepr., Am. Chem. Soc., Div. Polym. Chem.* **1979**, *20*, 558−561; *Chem. Abstr.* **1980**, *93*, 196819m.
[7] T. G. Gardner, G. S. Girolami, *Organometallics* **1987**, *6*, 2251−2256.
[8] T. G. Gardner, G. S. Girolami, *Angew. Chem. Int. Ed. Engl.* **1988**, *27*, 1693−1695.
[9] J. A. Jensen, S. R. Wilson, G. S. Girolomi, *J. Am. Chem. Soc.* **1988**, *110*, 4977−4982.
[10] P. Berno, S. Gambarotta, D. Richeson, in: *Comprehensive Organometallic Chemistry*, vol. II (Eds.: E. W. Abel, F. G. A. Stone, G. Wilkinson), Elsevier Science Ltd., Oxford, UK, **1995**.
[11] A. A. Danopoulos, P. G. Edwards, *Polyhedron* **1989**, *8*, 1339−1344.
[12] R. L. Bansemer, J. C. Huffman, K. G. Caulton, *Inorg. Chem.* **1985**, *24*, 3003−3006.
[13] J. Nieman, J. H. Teuben, J. C. Huffman, K. G. Caulton, *J. Organomet. Chem.* **1983**, *255*, 193−204.
[14] J. Lambe, C. Kikuchi, *Phys. Rev.* **1960**, *118*, 71−77.
[15] F. A. Cotton, J. Lu, *Inorg. Chem.* **1995**, *34*, 2639−2644.
[16] W. Plass, W. Schwarz, *Z. Anorg. Allg. Chem.* **1996**, *622*, 1756−1764.
[17] J. E. Drake, J. Vekris, J. S. Wood, *J. Chem. Soc. A* **1968**, 1000−1005.
[18] F. Montilla, A. Monge, E. Gutierrez-Puebla, A. Pastor, D. del Rio, N. C. Hernandez, J. F. Sanz, A. Galindo, *Inorg. Chem.* **1999**, *38*, 4462−4466.
[19] A. M. Arif, J. G. Heffner, R. A. Jones, B. R. Whittlesey, *Inorg. Chem.* **1986**, *25*, 1080−1084.
[20] L. R. Gray, A. L. Hale, W. Levason, F. P. McCullough, M. Webster, *J. Chem. Soc., Dalton Trans.* **1984**, 47−53.
[21] P. G. Edwards, J. S. Fleming, S. S. Liyanage, *J. Chem. Soc., Dalton Trans.* **1997**, 193−197.
[22] L. E. Manzer, *Inorg. Chem.* **1977**, *16*, 525−528.
[23] F. A. Cotton, M. P. Diebold, W. J. Roth, J. Wieslaw, *Polyhedron* **1985**, *4*, 1103−1108.
[24] G. Labauze, E. Samuel, J. Livage, *Inorg. Chem.* **1980**, *19*, 1384−1386.
[25] V. C. Gibson, T. P. Kee, R. M. Sorrell, M. McPartlin, *Polyhedron* **1988**, *7*, 2221−2223.
[26] P. G. Edwards, P. D. Newman, K. M. A. Malik, *Angew. Chem. Int. Ed.* **2000**, *39*, 2922−2924.
[27] P. G. Edwards, R. Haigh, M. L. Whatton, *Organometallics* **2000**, *14*, 2652−2654.
[28] P. G. Edwards, P. D. Newman, D. Hibbs, *Angew. Chem. Int. Ed.* **2000**, *39*, 2722−2724.
[29] L. E. Manzer, *Inorg. Synth.* **1982**, *21*, 135−139.
[30] S. F. Pedersen, J. B. Hartung, E. J. Roscamp, P. S. Dragovich, *Inorg. Synth.* **1992**, *29*, 119.
[31] D. F. Evans, *J. Chem. Soc.* **1959**, 2003−2005.
[32] J. W. Pflugrath, A. Messerschmidt, *MADNES*, version 11, Delft Instruments, Delft, **1989**.
[33] G. M. Sheldrick, *Acta Crystallogr., Sect. A* **1990**, *46*, 467−473.
[34] G. M. Sheldrick, University of Göttingen, **1993**.
[35] K. Davies, K. C. Prout, University of Oxford, **1993**.
[36] L. J. Farrugia, *ORTEP-3 for Windows*, University of Glasgow, **2001**.
[37] G. M. Sheldrick, *SHELX-97*, University of Göttingen, **1997**.
[38] N. P. C. Walker, D. Stuart, *Acta Crystallogr., Sect. A* **1983**, *39*, 158−166.

Received February 14, 2002
[I02077]